

Prediction of machining quality due to the initial residual stress redistribution of aerospace structural parts made of low-density aluminium alloy rolled plates

X. Cerutti¹ · S. Arsene² · K. Mocellin¹

Received: 21 February 2015 / Accepted: 20 July 2015 / Published online: 7 August 2015
© Springer-Verlag France 2015

Abstract During the machining of thick, large and complex aluminium parts, the redistribution of initial residual stresses is the main reason for machining errors such as dimensional variations and the post-machining distortions. These errors can lead to the rejection of the parts or to additional conforming operations increasing production costs. It is therefore a requirement to predict potential geometrical and dimensional errors resulting from a given machining process plan and in taking into consideration the redistribution of the residual stresses. A specific finite element tool which allows to predict the behaviour of the workpiece during machining due to its changing geometry and to fixture-workpiece contacts has been developed. This numerical tool uses a material removal approach which enables to simulate the machining of parts with complex geometries. In order to deal with industrial problems this numerical tool has been developed for parallel computing, allowing the study of parts with large dimensions. In this paper, the approach developed to predict the machining quality is presented. First, the layer removal method used to determine

the initial residual stress profiles of an AIRWARE[®] 2050-T84 alloy rolled plate is introduced. Experimental results obtained are analysed and the same layer removal method is simulated to validate the residual stress profiles and to test the accuracy of the developed numerical tool. The machining of a part taken from this rolled plate is then performed (experimentally and numerically). The machining quality obtained is compared, showing a good agreement, thus validating the numerical tool and the developed approach. This study also demonstrates the importance of taking into account the mechanical behaviour of the workpiece due to the redistribution of the initial residual stresses during machining when defining a machining process plan.

Keywords Residual stresses · Aluminium-Lithium alloy · Finite element · Machining · Dimensional and geometrical errors · Layer removal method

Introduction

Whether it is to improve the life time of the workpiece (mechanical strength, fatigue strength) or to optimise the manufacturing steps, the study of residual stresses and their effects on the mechanical behaviour of parts has become one of the major interests in the manufacturing industry. Residual stresses can be defined as self-equilibrated stresses existing in a solid material which is not submitted to any external load (thermal or mechanical). Sources of residual stresses can be decomposed into four different categories: the two first sources are the unequal plastic deformation resulting from mechanical and from thermal loads, the third one are metallurgical changes and the last one is a mismatch in the thermal expansion coefficients [4]. Manufacturing

✉ X. Cerutti
xavier.cerutti@mines-paristech.fr

K. Mocellin
katia.mocellin@mines-paristech.fr

¹ CEMEF - Centre for Material Forming, CNRS UMR 7635, Mines ParisTech, PSL - Research University, CS 10207 rue Claude Daunesse, 06904 Sophia-Antipolis Cedex, France, www.cemef.mines-paristech.fr

² Constellium Technology Center, 725 rue Aristide Bergès, CS 10027, 38341 Voreppe Cedex, France

processes being complex combinations of these sources, residual stresses cannot be totally avoided. Residual stresses are also categorised in three types in function of the length scale over which they act. Type I are macroscopic residual stresses, Type II are homogeneous microscopic residual stresses and Type III are heterogeneous microscopic residual stresses. In this study, only the residual stresses of Type I are considered.

The interest in mastering residual stresses and their effect is particularly high in aerospace [17]. The large monolithic aerospace parts are made from aluminium alloy rolled plates [11] or preformed parts (forged). These workpieces contain residual stresses which have been induced during the previous manufacturing steps. From the initial workpieces a significant amount of material is then removed by machining operations (usually by milling) to obtain the final functional parts. Up to 90 % of the initial volume of the part can be removed. In the most recent planes, the aluminium alloy parts account for about 20 % of the weight. Among these aluminium alloys, the new Al-Cu-Li alloys specifically developed for aeronautics and aerospace [12] are increasingly employed. It is therefore important to be able to master the residual stresses in these alloys and their effects on the machining quality.

In aerospace, machining is an essential step in the global manufacturing process of aluminium alloy parts. When a section of material is removed by machining, the initial residual stress equilibrium is broken and a new state of static mechanical equilibrium is thus achieved. The redistribution of residual stresses can induce displacements during machining, resulting in dimensional and geometrical errors. After removing the clamps the re-equilibrium of the part can provoke significant post-machining distortions. Both of these phenomena can lead to the non-conformity of the part with the dimensional and geometrical specifications.

In the past, several experimental and numerical studies on the influence of fixture [1, 13], cutting parameters [5–7] or machining sequences (tool path) [19] have been performed. In [15] the authors even present advanced FE models which take into account the thermomechanical loads linked to the tool-part interaction. In all of these models, the material removal is usually realised using a numerical method based on the deactivation of elements [23, 24]. This means that the material removal is based on the predefinition and the deactivation of a set of elements generated on the ideal machined path. The simulation of geometrically complex material removals on large parts (several meters) is then difficult with this numerical method. There is therefore a requirement of a numerical tool enabling to simulate the machining of such parts.

In order to understand and to control the machining process, a specific finite element tool allowing to simulate

machining sequences through massive material removal steps and to predict the machining quality by taking into consideration the redistribution of the initial residual stresses has been developed. It has been especially designed to study large and complex monolithic aeronautical parts made of aluminium alloys. This finite element tool is a computationally efficient numerical tool which enables to simulate the machining of parts in taking into consideration the influence of the coupled effect of the initial residual stress redistribution, the fixture and the machining sequence (tool path) [2]. The residual stresses created during machining are near-surface residual stresses [6]. When dealing with the machining of large and thick aluminium alloy parts they will thus be considered to be of second order compared to initial residual stresses [25]. Influences of cutting parameters are therefore not taken into account in this numerical tool.

Two main conditions are needed to accurately predict the machining quality: a computational tool allowing to simulate correctly the machining and a precise description of the workpiece residual stress state. The approach proposed in this article allows to predict accurately the workpiece behaviour during machining and thus the errors linked to this behaviour as well as the post-machining distortion by combining both of these conditions. The specific finite element tool has been developed based on the commercial version of FORGE[®]. FORGE[®] is a finite element software developed for material forming simulations. A P1+/P1 element with mixed velocity-pressure formulation is used [3]. The P1+/P1 is a linear element which possesses an additional degree of freedom for the velocity field which offers a good compromise between computational cost and accuracy of results. It is also compatible with an efficient automatic remeshing algorithm which makes it possible to deal with complex geometry description. In the first part of this article, a brief introduction of the specific parallel version of FORGE[®], which has been developed to simulate the machining of large and thick aluminium alloy aeronautical parts, is done. In the second part, the experimental results of the layer removal method, used to determine the initial residual stress profiles in rolled plates are analysed. The simulation of the layer removal method is presented and a comparison between experimental and simulation results is done as a first validation step. In the third part, a simulation to predict the machining quality of a part machined from a rolled plate is realised. The predicted dimensional errors as well as the post-machining distortion are then compared with experimental measurements. A good agreement is obtained between experimental and simulation results leading to a second validation and demonstrating the feasibility to predict accurately the machining quality using this approach and the specific numerical tool developed.

Finite element approach for the simulation of the machining process

The objective of the numerical tool is to predict the behaviour of the workpiece during machining in taking into consideration the redistribution of the residual stresses and thus the machining quality (geometrical and dimensional errors). In this finite element tool based on FORGE[®], the material removal is performed with a method using a Boolean deletion procedure [14]. This procedure allows to obtain the machined geometry by subtracting volumes from the current geometry of the workpiece. These volumes, which are described by surface meshes, represent the volume removed by the milling tool during a certain time (Δt) of the real machining sequence. They are automatically generated with a CAD/CAM software and the number of material removal steps is chosen by the user. It is important to point out that Δt is not necessarily constant and is usually chosen depending on the machining feature geometries (pockets, slots, holes, etc.) and the depth of cut.

The procedure is based on the computation of a signed distance between each node of the workpiece mesh and of the surface mesh representing the volume removed during one machining step. Depending on the sign of the distance, nodes are either removed or kept. When an element has nodes that should be removed and kept, the element is cut and new nodes and elements are created in order to obtain the new mesh. The machined parts are obtained after a relatively low number of massive removal steps.

This method has been chosen because the volume of material removed exactly represents the tool paths and therefore gives a good representation of the real machining. The workpiece deflections which can occur during the machining are taken into account. The volume of material removed during one step will therefore depend on the deflection of the workpiece observed after the previous step. The number of material removal steps used to describe the global removed volume during the machining sequence is chosen by the user, the higher the number of removal steps will be carried out the more detailed and accurate the simulation will be. Moreover, this technique is based on the use of an unstructured mesh composed of tetrahedral elements allowing to represent complex geometries. It requires remeshing after each machining step to increase the quality of the new mesh and field transfers (from the initial to the final mesh). The new mesh has therefore non-equilibrated fields (stress fields for example). The equilibrium is then computed on this new geometry to obtain the workpiece with its new residual stress state.

The parallel strategy used in this numerical tool involves SPMD modules (Single Program Multiple Data) and the MPI library (Message Passing Interface). This means that the initial mesh is divided into several mesh subdomains

(depending on the number of cores). Each core executes the same program and if needed, an exchange of information is performed between neighbouring cores. Figure 1 illustrates the three principal steps of a massive removal of material operation on a 2D mesh with two subdomains (two cores).

Using this approach, the developed numerical tool enables to simulate automatically complex machining operations and to predict the behaviour of the workpiece during the machining as well as the post-machining distortion. All necessary steps to simulate the removal of material are parallelized and automated. More details on the numerical methods used in this computational tool can be found in [2].

Determination of the residual stress profiles: the layer removal method

This part focuses on the layer removal method that was used to obtain the residual stress profiles of rolled plates. This method, introduced by [20], has as an objective to estimate residual stresses in sheet materials like rolled plates for example. The method is based on the successive removal of layers and on strain (or curvature) measurements (induced by the redistribution of the residual stresses after each removed layer). These operations are realised through the whole thickness of samples selected from a rolled plate. Using elastic theory the residual stress profiles inside the plate are then computed. However, this method is based on the following assumptions:

- 1/ Young's modulus and Poisson's ratio are constant in the specimens.
- 2/ The removal of successive layers does not disturb the initial residual stresses in the samples (no machining-induced residual stress).
- 3/ Residual stresses vary only throughout the thickness.

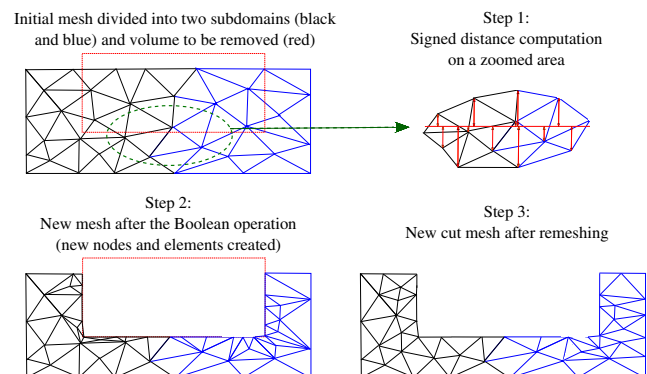


Fig. 1 The three principal steps to perform a massive removal of material on a mesh with boolean procedure (example in 2D on two cores)

For more information on the principle of the layer removal method using a strain gauge technique, interested reader can refer to the Appendix, where a description of a simplified example of layers removed from a panel is performed. The associated theoretical analysis allowing to relate the residual stress distribution to the measured strain is then briefly introduced. By presenting this method, the analysis of the redistribution of the initial residual stresses and the associated distortions during the removal of material is also explained.

A similar method developed by the Constellium Technology Center can be used on beams assuming that only one stress component is not equal to zero [9, 21]. This method has been chosen and is presented in the following section.

Results of the layer removal method

Using this method the residual stress profiles of a 70 mm thick AIRWARE® 2050-T84 alloy rolled plate selected for the tests have been determined. Successive removals of 3 mm-layers on two beams cut from the rolled plate are performed. One of the beam is taken from the rolling direction and the other from the transverse direction, as shown in Fig. 2a. The beams are chosen long enough (at least 5× the thickness of the plate) in order to avoid edge effects. After each removal, the beams are unclamped and strain measurements are performed, as illustrated in Fig. 2b.

Measures have been realised by the Constellium Technology Center using both strain gauges and indicators (distance amplifying instrument) in order to compare the measurements and to validate them. The successive layer removals are performed by machining, as shown in Fig. 3. To ensure that the machining does not disturb the initial

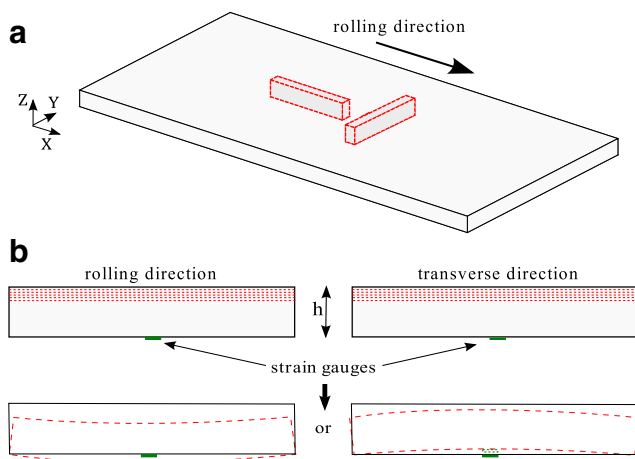


Fig. 2 Illustration of the layer removal on beams cut from rolled plates: **(a)** Beams taken from the middle of the plate to avoid all edge effects (350 × 30 × 70 mm) **(b)** Deformation which can be observed after layer removal and redistribution of the initial residual stresses



Fig. 3 The experimental set-up used to perform the layer removal method

residual stresses the smooth specific machining parameters summarized in Table 1 are used.

The machining of the successive layers on each beam as well as the strain measurements have then been performed. As explained in [9, 21], the average stress inside the i^{th} removed layer of the beams can then be computed for the layer 1 to $n - 1$ (with n the number of removed layers) using the measured strain and Eq. 1. $u(i)_{RD}$ and $u(i)_{TD}$ are the average stress in the removed layer i on the beam taken from the rolling direction (RD) and the transverse direction (TD) respectively.

$$\begin{aligned}
 u(i)_{RD} &= -E \frac{(\varepsilon(i+1)_{RD} - \varepsilon(i)_{RD})h^2(i+1)}{[h(i) - h(i+1)][3h(i) - h(i+1)]} - S(i)_{RD} \\
 u(i)_{TD} &= -E \frac{(\varepsilon(i+1)_{TD} - \varepsilon(i)_{TD})h^2(i+1)}{[h(i) - h(i+1)][3h(i) - h(i+1)]} - S(i)_{TD}
 \end{aligned}
 \tag{1}$$

with

$$\begin{aligned}
 S(i)_{RD} &= E \sum_{k=1}^{i-1} (\varepsilon(k+1)_{RD} - \varepsilon(k)_{RD}) \cdot \\
 &\quad \left[1 - \frac{3h(k)(h(i) + h(i+1))}{[3h(k) - h(k+1)]h(k+1)} \right]
 \end{aligned}$$

Table 1 Description of machining parameters

Tool diameter (mm)	63
Cutting speed (m/min)	280
Feed rate (mm/min)	400
Depth of cut (mm)	3

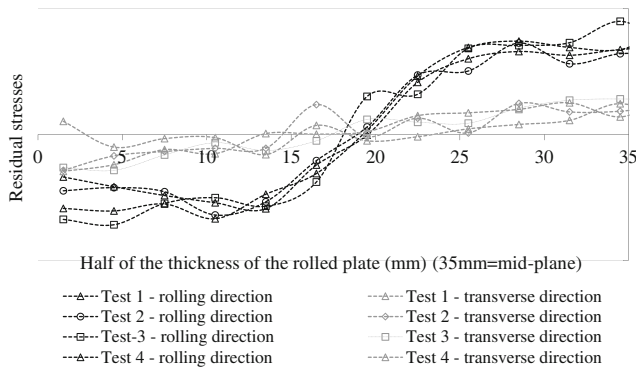


Fig. 4 Residual stress distributions obtained using the layer removal method with the strain gauge technique measurement

$$S(i)_{TD} = E \sum_{k=1}^{i-1} (\varepsilon(k+1)_{TD} - \varepsilon(k)_{TD}) \left[1 - \frac{3h(k)(h(i) + h(i+1))}{[3h(k) - h(k+1)]h(k+1)} \right]$$

with E being the Young’s modulus, $\varepsilon(i)$ the measured strain linked to the layer removal i and $h(i)$ the thickness of the beam before the layer removal i .

Using the two stress profiles in the beams computed with Eq. 1, the residual stress profiles in the rolled plate can be obtained using Eq. 2.

$$\begin{aligned} \sigma(i)_{RD} &= \frac{u(i)_{RD} + \nu u(i)_{TD}}{1 - \nu^2} \\ \sigma(i)_{TD} &= \frac{u(i)_{TD} + \nu u(i)_{RD}}{1 - \nu^2} \end{aligned} \quad (2)$$

with $\sigma(i)_{RD}$ and $\sigma(i)_{TD}$ being the initial residual stress profiles in the rolled plate and ν the Poisson’s ratio.

Twenty-two steps of layer removals have been performed to determine the residual stress profiles through the whole thickness of the beams taken from a 70 mm thick rolled plate. Experiments have been realised four times in each direction to analyse the repeatability and to validate the measurements. For some tests, the beams have also been taken from various positions in the plate (avoiding the position near the sides of the plates) to analyse an eventual deviation in the residual stress profiles depending on the position in the length of the plate (~ 7 m long). Figure 2 shows an example of the position of the beams in the rolled plate (a) and the different distortions which can be observed during the machining of the layers (b). The results obtained for the four tests are depicted in Fig. 4 and can be represented by the typical residual stress profiles shown in Fig. 5. Only one half of the residual stress profiles is illustrated along the thickness direction because of the symmetrical

distribution. Due to the low level of measured strain, the residual stress profiles in the transverse direction are more difficult to determine and thus present some fluctuations. However, relatively low deviations are visible between the different residual stress profiles in the rolling direction. Also only small deviations in the residual stress profiles depending on the position of the beams in the plates can be observed, showing a relatively low uncertainty in the residual stress profiles determination.

To characterise and evaluate the global residual stresses in a rolled plate, a specific indicator defined as the mean stored elastic energy per unit volume has been created [9, 11]. This stored elastic energy density W can be used to evaluate the potential risk of distortion (during and after the machining) and can be expressed as in Eq. 3.

$$W = \frac{1}{H} \int_0^H \frac{\sigma_{RD}^2 - 2\nu\sigma_{RD}\sigma_{TD} + \sigma_{TD}^2}{2E} \quad (3)$$

with W being the stored elastic energy density in kJ/m^3 and H the thickness of the plate.

Experience has shown that significant post-machining distortion could occur for materials containing a stored elastic energy density higher than $2 kJ/m^3$ [9]. This indicator enables therefore to give an order of magnitude of the distortion risk linked to the machining of a part taken from a rolled plate and to determine if particular attention has to be paid to the definition of the machining process plan. Note that the magnitude of the stored elastic energy density varies in function of the alloy but also in function of the thickness of the plate, the highest value usually being for a plate thickness range of 60–90 mm. For more information on the distortion risk, a stress range indicator (difference between the maximum and the minimum stress) can also be used. However, because the part geometry and its position within the workpiece are not taken into account in both of these indicators, no precise evaluation of distortion risk can be done [16]. Only the tendency of a product to distort after machining can be characterised.

The fact that the residual stress magnitude in the transverse direction is low shows that the total stored elastic

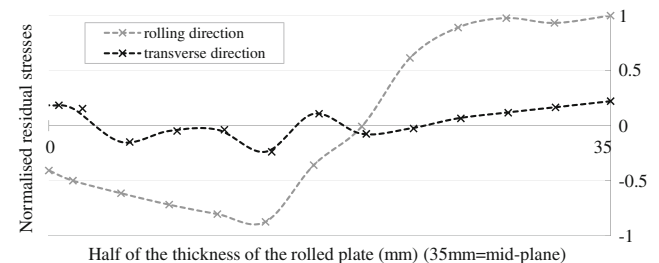
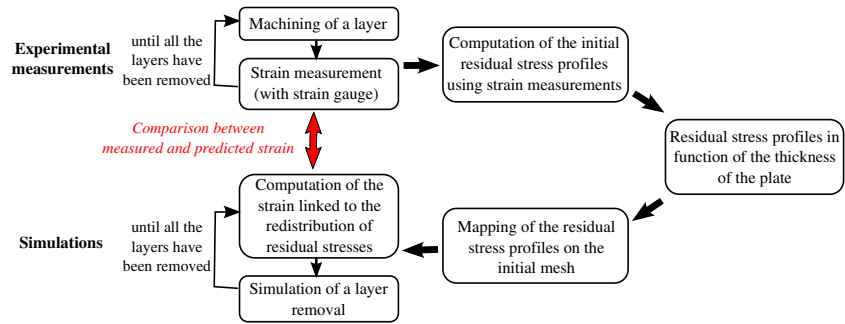


Fig. 5 Typical residual stress distribution of a 70 mm thick AIRWARE® 2050 alloy rolled plate (normalised residual stresses)

Fig. 6 Illustration of the simulation and the experimental analysis of the layer removal method



energy density is mainly due to the residual stresses in the rolling direction. The plate has therefore a strong anisotropy in its residual stress distribution.

The machining of a part selected from such a plate should thus have a low distortion if the initial workpiece is taken in the transverse direction whereas the risk of distortion is expected to be higher when dealing with workpieces taken in the rolling direction. In the case of large aeronautical parts, the parts are often too big to be machined in the transverse direction. The study of the behaviour of the workpiece due to the redistribution of the residual stresses during the machining is therefore of high importance.

Numerical simulations of machining

Simulation of the layer removal method

In order to evaluate the accuracy of the developed numerical tool [2] and of the residual stress profiles, a simulation of the layer removal method for the beam selected in the rolling direction has been performed. As illustrated in Fig. 6, in this simulation a reverse analysis of the layer removal experiment is done. As explained previously, this method has as an objective to use the measured strain to compute the initial residual stress profiles. In the simulation the residual stress profiles obtained experimentally and shown in Fig. 4 are used as input data. Then layer removals as well as the computation of the redistribution of the residual stresses and the associated strain are performed. Comparisons between experimentally measured strains (with strain gauge) and

predicted strains can thus be realised. Like for the experimental tests the initial specimens are 350 × 30 × 70 mm beams selected from a 70 mm thick rolled plate and the thickness of each removed layer is 3 mm. The mechanical properties of the alloy used in the simulations are summarized in Table 2.

In order to use the experimental residual stress profiles obtained as input data of the simulation, polynomial approximations have been done. Figure 7 shows the polynomial functions used to describe the residual stress profiles in Fig. 5. Using a specific script, the residual stress profiles are then computed on the initial mesh using the coefficients of the polynomial functions determined previously. The initial mesh with initial residual stress fields is obtained in this way. No distortion of the mesh can be observed during the computations of the residual stress profiles on the initial mesh, which proves that the initial residual stress profiles are balanced.

The initial mesh is an unstructured mesh composed of tetrahedral elements (P1+/P1). Due to the formulation used in FORGE® the stress fields are P0 variables (constant per element). To ensure a good description of the variation of residual stresses through the thickness and an accurate computation of the strain field a small mesh size has been defined. As shown in Fig. 8a, the initial element size used is 1.25 mm which represents a mean of 56 elements along the

Table 2 Main mechanical properties of the AIRWARE® 2050-T84 alloy used in the simulations

Young’s modulus (E)	75000 MPa
Poisson’s ratio (ν)	0.33
Density (ρ)	2693 kg/m ³
Tensile Yield Strength	500 MPa

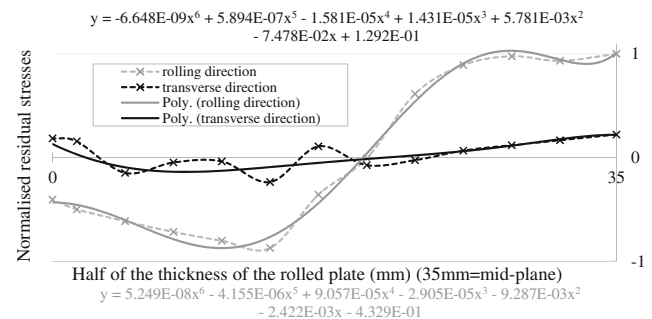


Fig. 7 Polynomial functions used to apply the residual stress profiles on the initial mesh (normalised residual stresses)

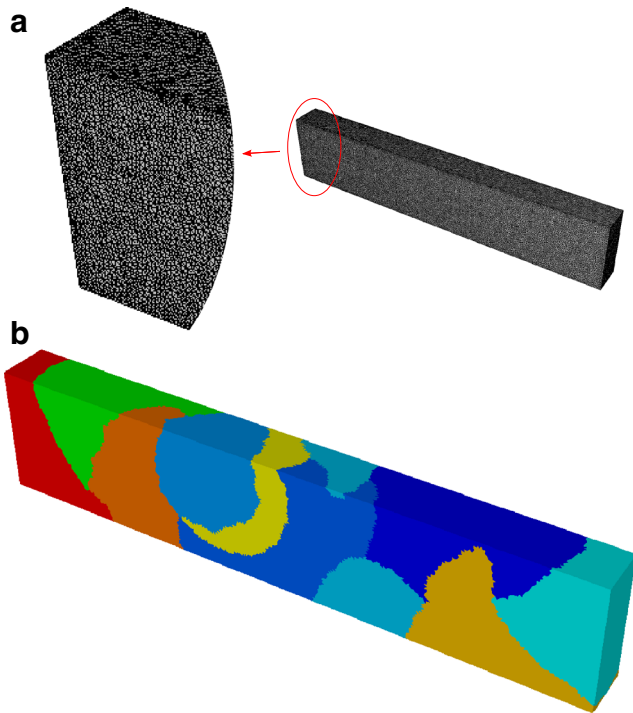


Fig. 8 Initial mesh: **a** Initial mesh composed of about 407,000 nodes and 2,269,000 tetrahedral elements, **b** Initial mesh subdomains (parallel computation: simulation launched on 10 cores)

total thickness (70 mm). Depending on the removed volume, a new size of mesh is computed at each remeshing step. The objective is to ensure a certain number of elements in the thickness during the whole simulation.

To avoid perturbation in the initial residual stresses clamping forces must be low. Clamping can therefore be modelled by simply restricting degrees of freedom (DoF) of nodes in contact with clamps. After each layer removal the clamping condition is removed and strains linked to the redistribution of the residual stresses are computed. Figure 9 is a simplified flow chart of the procedure of the simulation of the layer removal method.

Simulations have been performed on ten cores, the mesh thus being divided automatically in ten subdomains. For each removal step a new mesh and then new subdomains are obtained. Subdomains are automatically regenerated to ensure that each core runs the same amount of nodes, as shown in Fig. 8b. Twelve steps of layer removal have been simulated. A numerical sensor has been positioned on the mesh at the strain gauge location, as illustrated in Fig. 2b. For each removed layer the evolution of the elastic strain, shape of the beam (distortion) and the residual stress state is obtained, as shown in Fig. 10.

Results in terms of strains obtained for all twelve removals are depicted in Fig. 11. A good agreement between

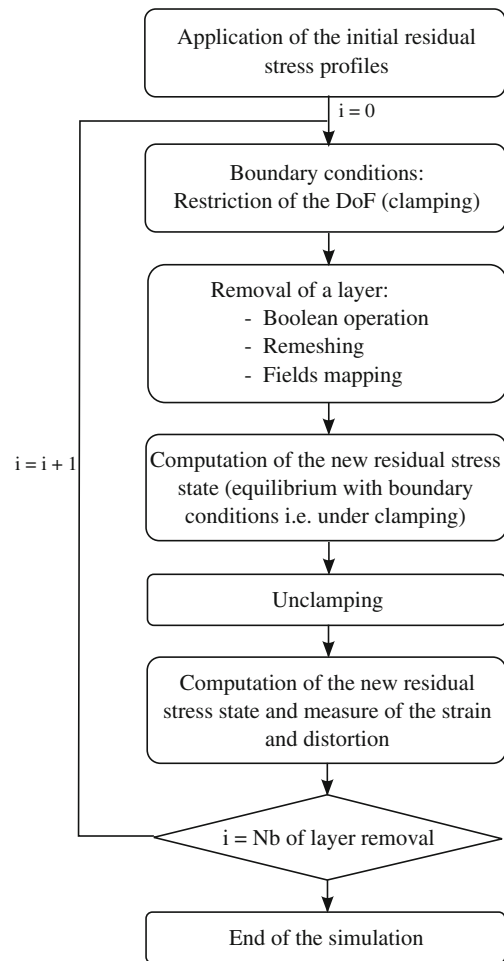


Fig. 9 Flow chart of the simulation of the layer removal method procedure

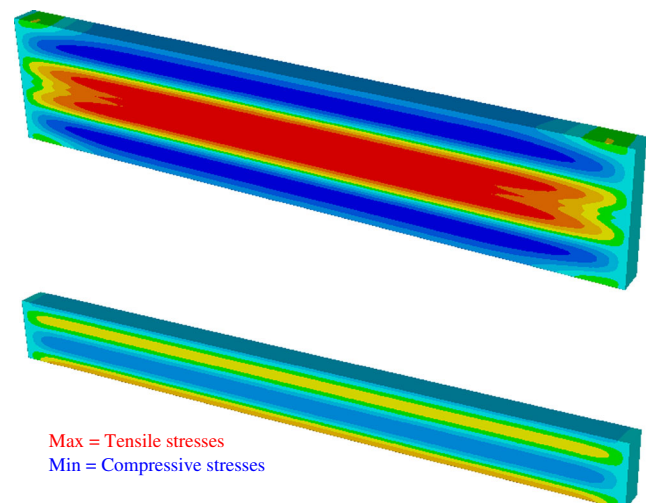
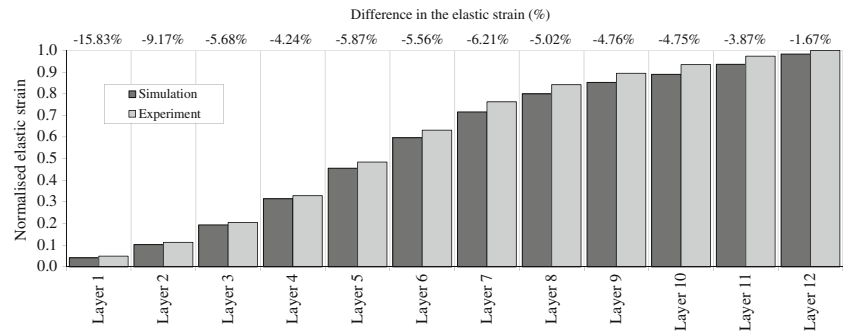


Fig. 10 Evolution of the longitudinal residual stress field. Comparison between the initial residual stress field and the one after 12 material removing steps

Fig. 11 Evolution of the elastic strain during the layer removal method (normalised elastic strain). Comparison of simulation and experimental results. The difference in the elastic strain obtained by simulation and experiment in percent is also depicted.



experimental and simulation strains is achieved. The difference between measured and predicted strains stays under 10 % (except for the first layer where the strain is very low) with a majority even close to 5 %. The evolution of the curvature of the beam for each removal step can be observed in Fig. 12. The cross represents the maximum displacement observed experimentally after the first twelve steps. A maximum value of 0.33 mm for the predicted and 0.32 mm for the experimental test is obtained, which represents a difference of only 3 %. The final predicted distortion is thus similar to what has been observed experimentally. Moreover we can also observe a bigger increase of the curvature during the layer removals 4 to 8. These layers correspond to the area of a bigger gradient of the initial residual stress profiles.

With the simulation of the layer removal experiment the approach coupling the developed finite element tool and a method to determine accurately the residual stress profiles has been validated. The predicted and measured strains show similar trends over the entire layer removal test. Knowing the initial residual stresses, the developed numerical tool therefore enables to predict the redistribution of the initial residual stresses and the associated distortions.

Simulation of machining of a part: machining quality prediction and comparison with experimental results

In this section, the numerical tool is used to simulate the machining of a part. The machining quality predicted

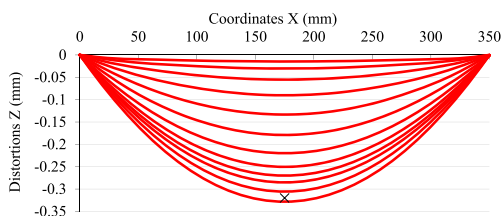


Fig. 12 Evolution of the curvature of the specimen during the twelve removals of layers. The cross represents the maximum displacement observed experimentally after the twelfth layer removal

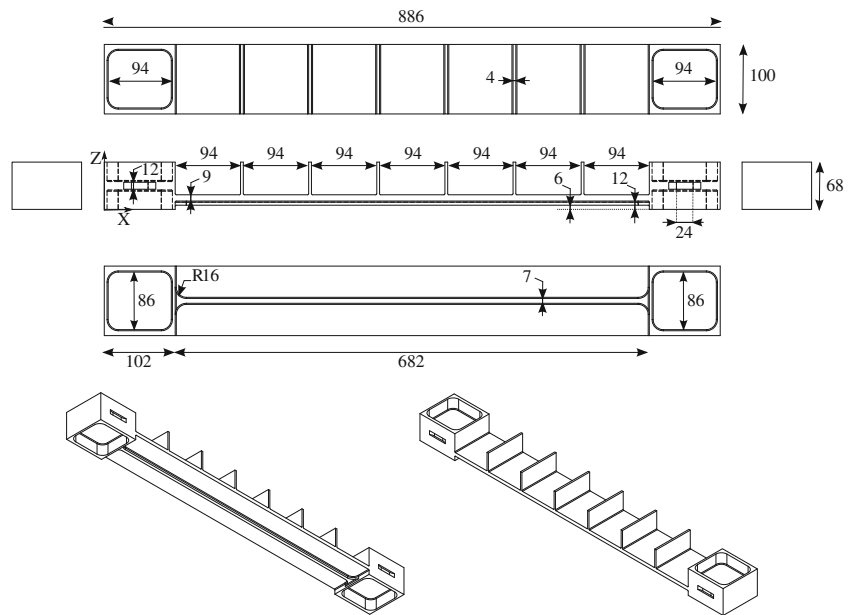
(post-machining distortion and dimensional errors) is then compared with experimental results. The part considered is presented in Fig. 13. It is not an aeronautical part and has been designed to evaluate the approach and the developed numerical tool in a case of machining of an aluminium alloy part. Almost 80 % of the volume of the initial workpiece is removed during the machining, which is representative of the amount of material usually machined in aeronautics.

The initial workpiece is $886 \times 100 \times 70$ mm and is taken in the rolling direction from the rolled plate studied in section “Simulation of the layer removal method”. The residual stress field is obtained as explained in section “Simulation of the layer removal method”. Then one millimetre on both the upper and lower part of this block is removed and four clamping grooves of $24 \times 4 \times 14$ mm on the sides of the workpiece are machined to obtain the prepared geometry shown in Fig. 14.

With the preparation step, the so-called initial workpiece with its residual stress fields has been created. Two machining steps are then required to obtain the final part geometry introduced above. The first machining step consists in the machining of the machining features (two pockets and the longitudinal rib) located on the bottom surface of the workpiece ($Z = 0$ mm). Based on the numerical approach, the material removed during this machining step has been discretized in eleven layer removal steps. When this first machining step is finished, the workpiece is flipped to perform the second machining step. This step, where most of the material is removed, has been discretized in fifty-seven layer removal steps. Before each simulation of a machining step, the clamping of the workpiece is simulated to obtain the effect of the clamping on the residual stress state and on the geometry. The workpiece is positioned with the help of three locators fixed on the table and is maintained in position with four clamps with a controlled force of 11 kN each. The fixture layout used for the simulation can be seen in Fig. 15.

In the simulation, clamps, locators and the table are considered as rigid bodies to simplify the model and therefore

Fig. 13 The case studied: geometry of the machined part



to reduce the computation time. However, clamping systems could also be modelled as deformable bodies with this numerical tool. The workpiece-fixture contact is taken into account using a penalty method already existing in FORGE® [8]. The friction model used is a Coulomb limited Tresca Law defined as in Eq. 4 with $\mu = 0.45$ and $\bar{m} = 0.6$. These values have been chosen to represent the contact between the fixture elements made of steel and the workpiece made of aluminium alloy.

$$\begin{aligned} \tau &= \mu\sigma_n \text{ if } \mu\sigma_n < \bar{m} \frac{\sigma_0}{\sqrt{3}} \\ \tau &= \bar{m} \frac{\sigma_0}{\sqrt{3}} \text{ if } \mu\sigma_n \geq \bar{m} \frac{\sigma_0}{\sqrt{3}} \end{aligned} \quad (4)$$

with μ being the Coulomb’s friction coefficient, \bar{m} the Tresca friction coefficient (comprised between 0 and 1), σ_n being the contact pressure, τ the shear stress and σ_0 the yield strength of the material.

The machining sequence used in this case is the one presenting the smallest machining time, that is to say the one allowing to minimise the tool path length. For both machining steps, the material removals are therefore performed starting at one side of the part ($X = 0$ mm) ending at the other ($X = 886$ mm). The material removal depth of each

layer is defined in function of the real machining depth of cut. All geometries of the volume removed have been automatically generated using a CAD/CAM software and are therefore easily and quickly obtained from a machining programme.

The initial mesh is composed of about 930,000 nodes and 5,250,000 elements and computations have been realised on twelve cores. Figure 16 shows the evolution of the XX stress tensor component and of the displacements along the z-axis which can be observed during the machining simulation at three different steps of the first machining step. In the same way, the evolution of the XX stress tensor component and of the displacements along the z-axis observed during the machining simulation at five different steps of the second machining step are depicted in Fig. 17.

In parallel, experimental machining has been performed. The part has been machined with the same machining process plan described for the simulation (depth of cut, radius of the tool, fixture layout and machining sequence).

The machining quality has been evaluated by performing two types of measurements. The first one is the post-machining distortion, which is evaluated after each



Fig. 14 The case studied: prepared workpiece

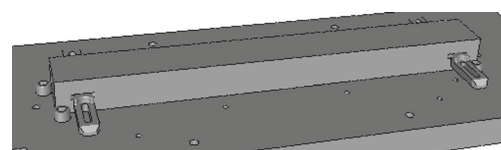
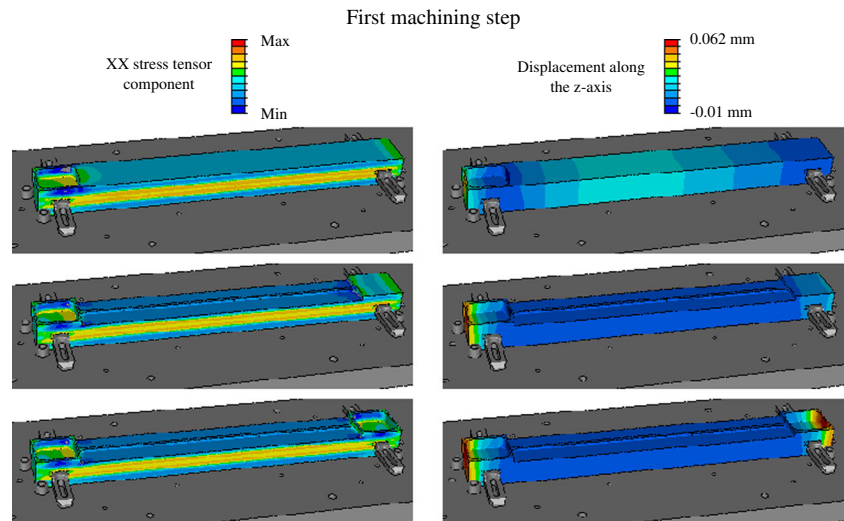


Fig. 15 The fixture layout used for the simulation of machining [2]

Fig. 16 Evolution of the workpiece geometry during the first machining: the residual stress state (XX stress tensor component) and the displacements along the z-axis linked to the changing geometry of the workpiece during the machining simulation and the residual stress redistribution



machining step (after the unclamping). The post-machining distortion represents the curvature of the part and is measured on the top and bottom surfaces. The second criterion is the dimensional variations (undercuts and overcuts), which represent the machining accuracy. They are evaluated by

measuring the thickness variations of the wall (parallel to the top and bottom surfaces of the workpiece) with a nominal dimension of 12 mm for the pockets located at each end of the part and 9 mm for the pockets located in the middle. Experimentally, the measurements have been performed

Fig. 17 Evolution of the workpiece geometry during the second machining: the residual stress state (XX stress tensor component) and the displacements along the z-axis linked to the changing geometry of the workpiece during the machining simulation and the residual stress redistribution

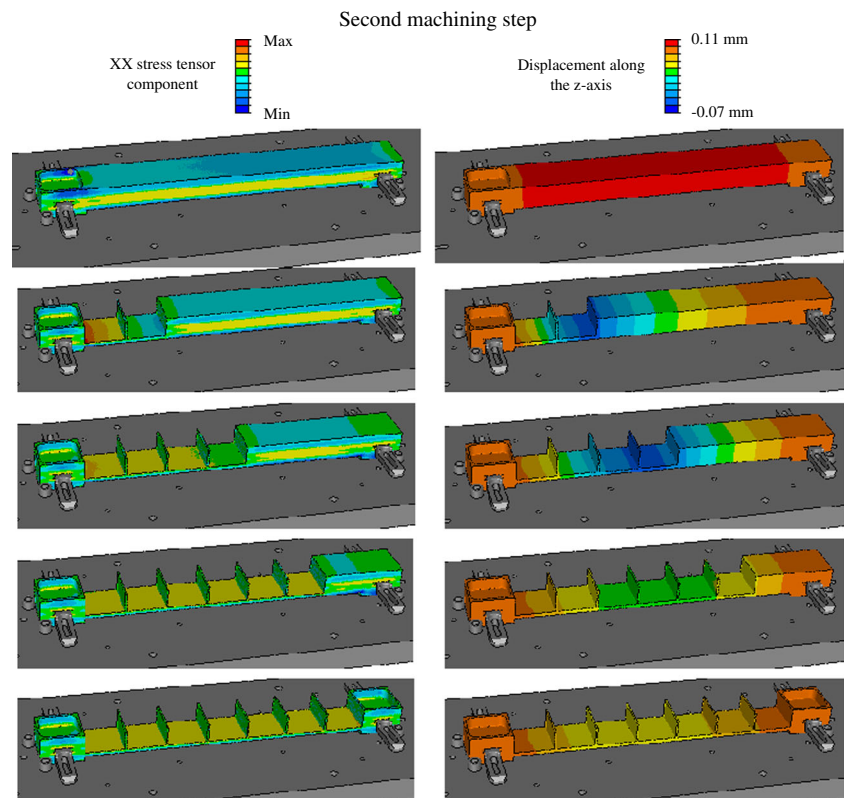
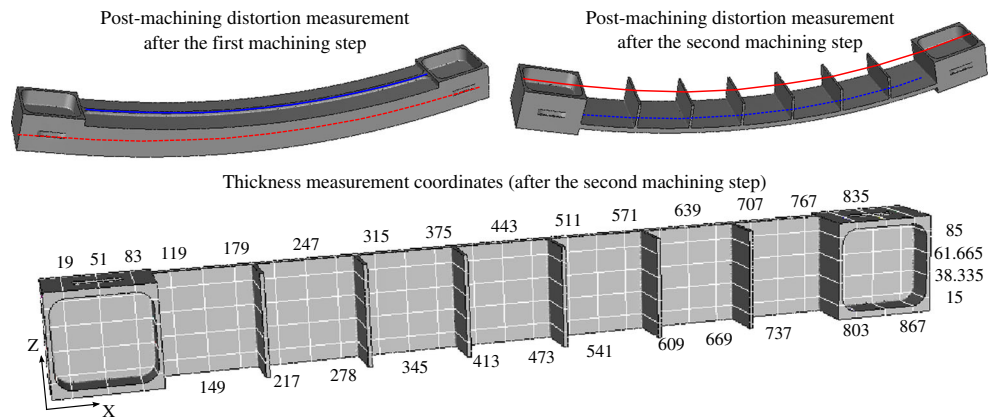


Fig. 18 The machining quality evaluation: post-machining distortions (the blue and red lines represent the measurements performed on the bottom and top surfaces respectively) and coordinates of the thickness measurements



using a coordinate-measuring-machine (CMM). Both types of measurement are illustrated in Fig. 18.

The results obtained in terms of post-machining distortions for both machining steps are depicted in Fig. 19. A good agreement between the numerically predicted post-machining distortions and the measured ones can be observed, demonstrating the capability of the developed approach to predict accurately the residual stress state and associated distortions after each machining step.

The results obtained in terms of the variation of thickness (machining accuracy) at the end of the machining are

showed in Fig. 20. A good agreement between the numerically predicted overcuts/undercuts and the measured ones is achieved, demonstrating also the capability of the developed approach to predict accurately the evolution of the residual stress state in the workpiece and its associated deflections during the whole machining process. Mainly undercuts are observed in this case, which means that the wall thickness is bigger than the one aimed for. These undercuts are the results of the deflections which can be observed during the machining in Fig. 17 (mainly negative deflections).

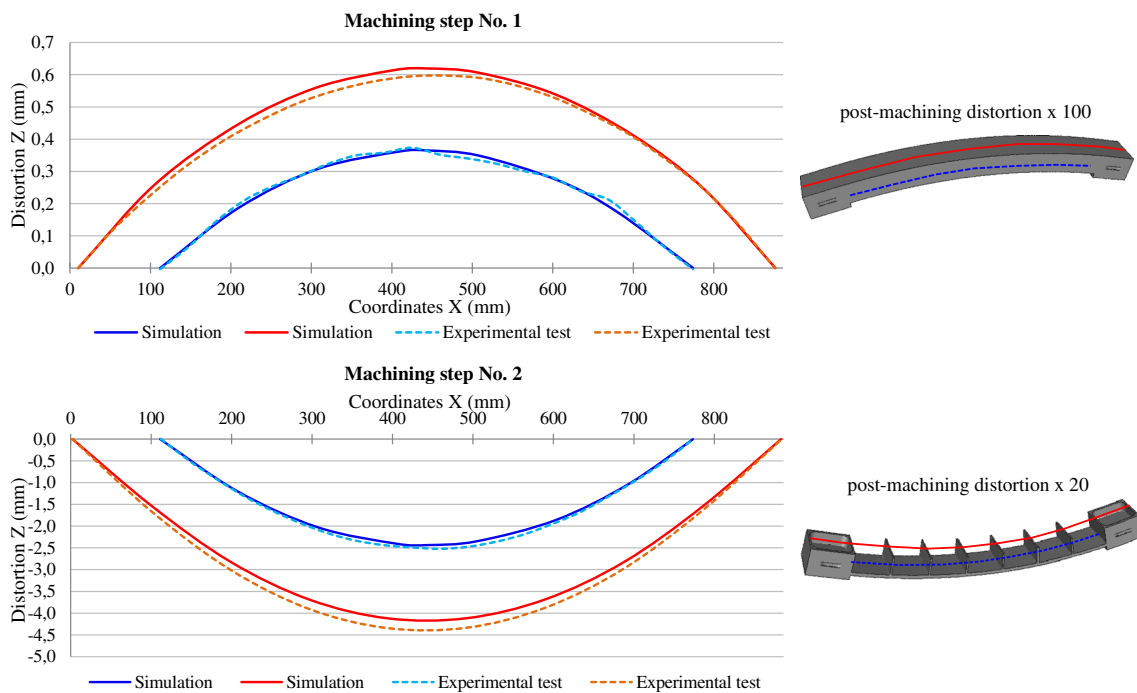
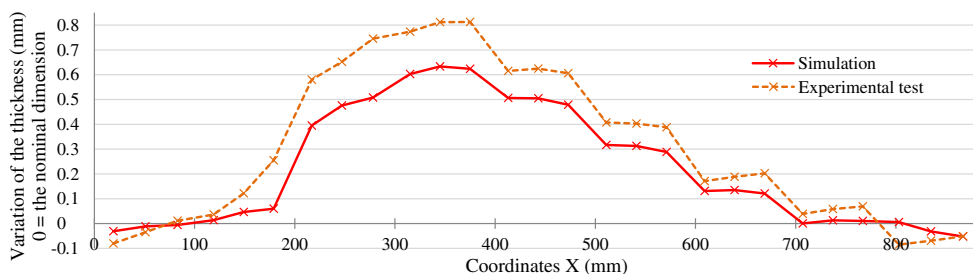


Fig. 19 The post-machining distortion of the part: comparison between experimental and simulation results

Fig. 20 Variation of thickness of the wall with a nominal dimension varying from 12 mm to 9 mm (0 = nominal dimension): comparison between experimental and simulation distortion



Conclusion and outlook

In this paper, the influence of residual stresses inside blocks of material taken from an aluminium alloy rolled plate on the machining distortion is studied. In a first step, the layer removal method with strain gauge measurements used to determine residual stress profiles in a rolled plate is presented. The residual stress profiles of a 70 mm thick rolled plate have then been obtained with this method. The residual stress distribution shows that depending on the geometry of the part and on manufacturing conditions, workpiece deflections during the machining as well as post-machining distortions of parts made from a 70 mm thick rolled plate could occur.

In a second step, using the developed numerical tool [2] a simulation of the layer removal method has been performed. A good agreement between experimentally measured strains and predicted strains is obtained, validating the approach on which the developed numerical tool is based as well as the method to determine the initial residual stress profiles.

In the last part of this paper, an example of a simulation for the prediction of the machining quality of a machined part is performed. The predicted machining quality of the part is similar to the experimental one both in terms of post-machining distortion and dimensional errors. This example shows the validity of the developed numerical tool which enables to predict the workpiece deflections during machining and the post-machining distortion in function of the initial residual stress state, the geometry desired, the machining sequence and the fixture layout.

Based on the approach presented in this paper and on the use of numerical tools as the one developed in the framework of this project, it is possible to predict dimensional and geometrical errors due to the redistribution of the residual stresses during machining. The use of such an approach therefore gives the possibility to validate a machining process plan before going into real machining and to optimise it. Using this numerical tool, studies on the prediction of the machining quality (post-machining distortions as well as dimensional and geometrical errors) and the influence of the various parameters will thus be performed in the future.

Acknowledgments This work is done in the framework of the OFELIA project, labelled by the “ViaMéca Competitiveness Cluster”, gathering several industrial partners (Constellium, Aubert & Duval and REXIAA) and research laboratories (IFMA, SPIN and CEMEF). The authors are thankful for the financial aid to this project supplied by the French Ministry of Industry and also thank S. Hassini and Prof. E. Duc from IFMA for the experimental machining tests and all the partners of this project for their help and collaboration.

Appendix: The redistribution of the residual stresses and the principle of the layer removal method

Let *h* and *b* denote respectively the height and width of a panel sampled from a rolled plate. A strain gauge has been bonded to it. Assuming plane stress conditions ($\sigma_{zz} = 0$), the strains ϵ_{xx} and ϵ_{yy} in the *x*- and *y*-directions can be expressed as

$$\epsilon_{xx} = \frac{\sigma_{xx} - \nu\sigma_{yy}}{E} \quad \epsilon_{yy} = \frac{\sigma_{yy} - \nu\sigma_{xx}}{E} \tag{5}$$

where σ_{xx} and σ_{yy} are the stresses in the *x*- and *y*-directions.

In order to simplify the problem presented in this introduction, the assumption that $\sigma_{xx} = \sigma_{yy} = \sigma(z)$ is made. $\sigma(z)$ therefore represents the residual stress profiles which evolve only through the thickness of the plate. Using this assumption the strains in both the *x*- and *y*-directions are given by

$$\epsilon(z) = \frac{(1 - \nu)\sigma(z)}{E} \tag{6}$$

The forces and bending moments associated with the initial residual stress profiles being balanced, the following conditions can be written

$$\begin{aligned} F_x = F_y = b \int_0^h \sigma(z) dz &= 0 \\ M_x = M_y = b \int_0^h \sigma(z) z dz &= 0 \end{aligned} \tag{7}$$

with F_x and F_y being the forces and M_x and M_y the bending moments in the *x*- and *y*-directions.

When the material is removed layer by layer, a new state of equilibrium is reached and therefore a new residual stress

profile is obtained. If one layer with a thickness of a is removed, the new residual stress σ' can be expressed as

$$\sigma'(z) = \sigma(z) + \sigma_{I1}(a) \tag{8}$$

with $\sigma_{I1}(a)$ being a uniform balancing stress due to the removal of the first layer.

Considering balanced forces in the resulting specimen, the following equation can be written

$$b \int_0^{h-a} \sigma'(z) dz = 0 \tag{9}$$

Whereas the forces will be balanced, the bending moments will not be, due to the new asymmetric residual stress profile. A moment has to be created to counterbalance the moment $M(a) = b \int_0^{h-a} \sigma'(z) z dz \neq 0$ [22]. The new residual stress profile that will satisfy both the force and moment equilibrium can be written as

$$\sigma_{new}(z) = \sigma'(z) + \frac{M(a) \left(\frac{h-a}{2} - z\right)}{I} \tag{10}$$

with I the moment of inertia expressed as

$$I = \frac{b \times (h - a)^3}{12}$$

The sample will deform due to the redistribution of the residual stresses and due to the re-equilibrium of the forces and moments. Figure 21 illustrates the evolution of the residual stress profile, starting from the initial residual stress profile $\sigma(z)$ to the residual stress profile allowing to obtain the force equilibrium $\sigma'(z)$ and then the residual stress profile allowing to fulfil both the force and moment equilibrium $\sigma_{new}(z)$. It is the re-equilibrium of the moment which will then provoke distortions as also illustrated in Fig. 21.

The strain gauge is used to measure the strain linked to the redistribution of the residual stresses. It is bonded to the center of the lower surface of the sample and measures the evolution of the strain after each removal of a layer. Using this method, authors in [10, 18, 22] have demonstrated that it is possible to link the initial residual stress profiles to the measured strain. Equation 11 represents this relation and gives the measured strain depending on the thickness of the layer removed. For more details on this technique and the theoretical analysis, readers can refer to [18, 22].

$$\varepsilon(a) = \frac{1 - \nu}{E(h - a)^2} \int_0^{h-a} [6z - 4(h - a)] \sigma(z) dz \tag{11}$$

with $\varepsilon(a)$ being the strain detected by the strain gauge due to the removal of a layer of thickness a and $\sigma(z)$ the initial residual stress profile.

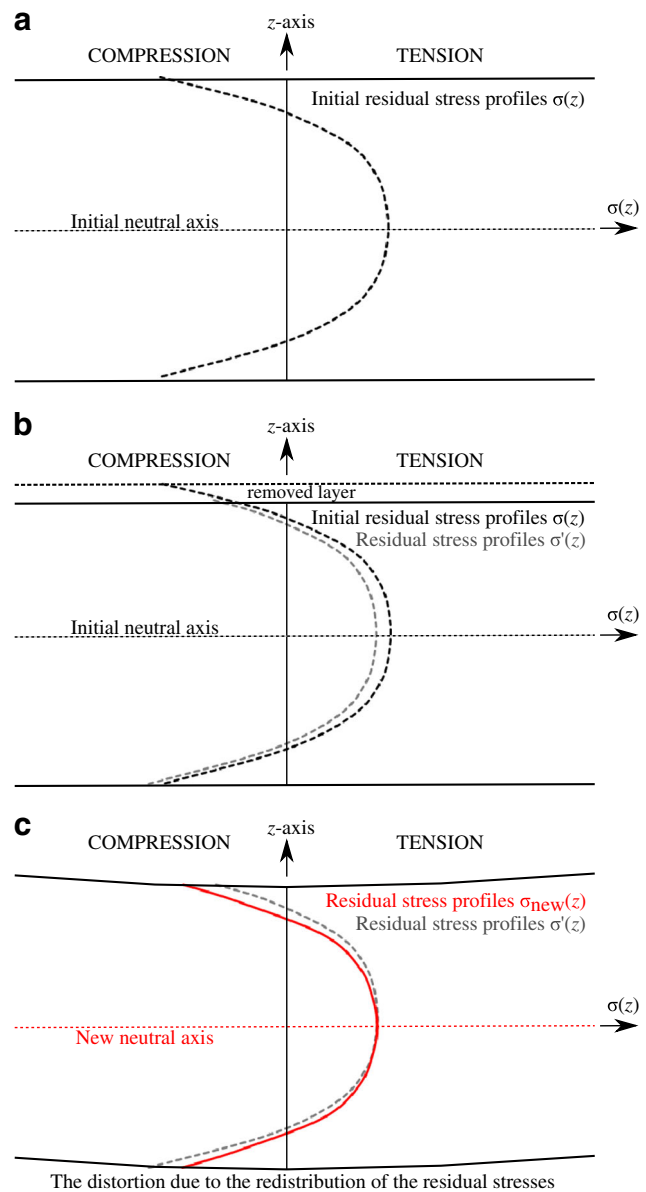


Fig. 21 Illustration of the residual stress redistribution after the removal of a layer with a simplified residual stress distribution: (a) the initial residual stress profile (b) the residual stress profile after the layer removal with only balanced forces (c) the new residual stress profile after the layer removal respecting both force and moment equilibrium

References

- Asante J (2008) A combined contact elasticity and finite element-based model for contact load and pressure distribution calculation in a frictional workpiece–fixture system. *Int J Adv Manuf Technol* 39(5–6):578–588
- Cerutti X, Mocellin K (2014) Parallel finite element tool to predict distortion induced by initial residual stresses during machining of aeronautical parts. *Int J Mater Form*. doi:10.1007/s12289-014-1164-0
- Chenot J (1989) Three dimensional finite element modeling of forging process. In: *Computational Plasticity: Models, Software*

- and Applications, pp. 793–816. Proceedings of the Second International Conference Held in Barcelona
4. Das S, Chandra U (1999) “Residual stress and distortion,” in handbook of aluminum metallurgy: processes and equipment, vol 1. G.E. Totten and D.S. Mackenzie, Marcel Dekker, Inc., New York
 5. Denkena B, Boehnke D, Len L (2008) Machining induced residual stress in structural aluminum parts. *Prod Eng* 2(3):247–253
 6. Denkena B, Leon LD (2009) Milling induced residual stresses in structural parts out of forged aluminium alloys. *Int J Mach Mater* 4(4):335–344. doi:[10.1504/IJMMM.2008.023717](https://doi.org/10.1504/IJMMM.2008.023717)
 7. Denkena B, de Leon Garcia L (2007) Fem-simulation of high-performance-milling. In: Proceeding of the CIRP Conference on modelling of machining operations, Sicily
 8. Fourment L, Chenot JL, Mocellin K (1999) Numerical formulations and algorithms for solving contact problems in metal forming simulation. *Int J Numer Methods Eng* 46(9):1435–1462
 9. Heymes F, Commet B, Dubost B, Lassince P, Lequeu P, Raynaud GM (1997) Development of new al alloys for distortion free machined aluminium aircraft components. *ASM International(USA)*, 249–255
 10. Jeanmart P, Bouvaist J (1985) Finite element calculation and measurement of thermal stresses in quenched plates of high-strength 7075 aluminium alloy. *Mater Sci Technol* 1(10):765–769
 11. Lequeu P, Lassince P, Warner T, Raynaud GM (2010) Engineering for the future: weight saving and cost reduction initiatives. *Aircraft Engineering and Aerospace Technology* 73:147–159
 12. Lequeu P, Smith K, Danielou A (2010) Aluminum-copper-lithium alloy 2050 developed for medium to thick plate. *J Mater Eng Perform* 19(6):841–847
 13. Li B, Melkote SN (1999) Improved workpiece location accuracy through fixture layout optimization. *Int J Mach Tools Manuf* 39(6):871–883
 14. Ma K, Goetz R, Svrivatsa S (2010) Modeling of residual stress and machining distortion in aerospace components. *ASM Handbook, Metals Process Simulation* 22B:386–407
 15. Rai JK, Xirouchakis P (2008) Finite element method based machining simulation environment for analyzing part errors induced during milling of thin-walled components. *Int J Mach Tools Manuf* 48(6):629–643
 16. Schultz R, Karabin M (2002) Characterization of machining distortion by strain energy density and stress range. In: 6th European conference on residual stresses, Materials Science Forum, vol 404–407, pp 61–68
 17. Sim W (2010) Challenges of residual stress and part distortion in the civil airframe industry. *Int J Microstruct Mater Prop* 5:446–455
 18. Tandon R, Green DJ (1990) Residual stress determination using strain gage measurements. *J Am Ceram Soc* 73(9):2628–2633
 19. Tang ZT, Liu ZQ, Ai X (2007) Optimization of bulkhead processing sequence for multi-frame monolithic components by fem. *Adv Mater Res* 24–25:355–360
 20. Treuting RG, Read WTJ (1951) A mechanical determination of biaxial residual stress in sheet materials. *J Appl Phys* 22(2):130–134
 21. Van Der Veen S, Heymes F, Boselli J, Lequeu P, Lassince P (2006) Low internal stress al-zn-cu-mg plates. *US Patent App.* 11/299, 683
 22. Virkar AV (1990) Determination of residual stress profile using a strain gage technique. *J Am Ceram Soc* 73(7):2100–2102
 23. Wang SP, Padmanaban S (2004) A new approach for fem simulation of nc machining processes. *AIP Conf Proc* 712(1):1371–1376. doi:[10.1063/1.1766720](https://doi.org/10.1063/1.1766720)
 24. Wei Y, Wang X (2007) Computer simulation and experimental study of machining deflection due to original residual stress of aerospace thin-walled parts. *Int J Adv Manuf Technol* 33(3–4):260–265. doi:[10.1007/s00170-006-0470-1](https://doi.org/10.1007/s00170-006-0470-1)
 25. Yang Y, Li M, Li K (2013) Comparison and analysis of main effect elements of machining distortion for aluminum alloy and titanium alloy aircraft monolithic component. *Int J Adv Manuf Technol*:1–9. doi:[10.1007/s00170-013-5431-x](https://doi.org/10.1007/s00170-013-5431-x)